International Journal of Minerals, Metallurgy and Materials
Volume 27, Number 9, September 2020, Page 1234
https://doi.org/10.1007/s12613-020-2023-2

Effect of flash processing on recrystallization behavior and mechanical performance of cold-rolled IF steel

Peng-yu Wen[1,2], *Jian-sheng Han*[1], *Hai-wen Luo*[1,2], *and Xin-ping Mao*[1]

1) State Key Laboratory of Advanced Metallurgy, University of Science and Technology Beijing, Beijing 100083, China
2) Department of Ferrous Metallurgy, University of Science and Technology Beijing, Beijing 100083, China
(Received: 1 December 2019; revised: 13 February 2020; accepted: 17 February 2020)

Abstract: Flash processing (FP) has attracted considerable attention due to its high efficiency, economic advantages, and the extraordinary opportunity if offers to improve the mechanical properties of steel. In this study, we investigated the influences of FP on the recrystallization (REX) behavior and mechanical performance of cold-rolled IF steel. Using a thermomechanical simulator, we performed both single-stage FPs, at heating rates of 200°C/s and 500°C/s, and two-stage FP, with an initial preheating to 400°C at a rate of 5°C/s and then to peak temperatures at a rate of 200°C/s. In comparison to continuous annealing (CA), single-stage FP can effectively refine the recrystallized grain sizes and produce a similar or even sharper γ (ND (normal direction)//{111}) texture component. In particular, the heating rate of 500°C/s led to an increase in the yield strength of about 23.2% and a similar ductility. In contrast, the two-stage FP resulted in a higher REX temperature as well as a certain grain refinement due to the stored strain energy, i.e., the driving force of REX, which was largely consumed during preheating. Furthermore, both stronger {110}<110> and weaker γ texture components appeared in the two-stage FP and were believed to be responsible for the early necking and deterioration in ductility.

Keywords: flash processing; interstitial-free steel; recrystallization; mechanical properties; texture

1. Introduction

Interstitial-free (IF) steel is an irreplaceable advanced-high-strength steel (AHSS) used in the automotive industry, in which atoms of the interstitial elements C and N are scavenged upon the addition of elements Ti or Nb [1]. It is well known that this steel possesses excellent formability and superior deep drawability due to the existence of strong γ (ND (normal direction)//{111}) fiber recrystallization (REX) texture [2–4], so it has been extensively used in the outer shells of cars [5]. In the past decade, considerable efforts have been made to achieve extremely low C and N contents by optimized metallurgical processing [6–7] to further improve drawability, as a stronger and more ductile IF steel is now in demand due to the requirement for lightweight automobiles. For example, using extra mechanical deformation processes, heterogeneous microstructures have been formed [8–10] that could be used to manufacture stronger IF steel due to the mechanical incompatibility of the gradient layers. However, the commercialization of these advances has met with great difficulty.

Flash processing (FP) has emerged as one of the most promising methods for developing stronger AHSS steel via grain refinement with unprecedented high efficiency [11]. However, due to the induced high thermal stress, the scale-up of FP to industrial product sizes can cause large distortion in the thin flat product. As such, a preheating stage is often included to minimize the temperature gradient [12]. There is ongoing controversy regarding how the heating rate and preheating stage could affect the REX and mechanical properties of cold-rolled IF steel, with no universally accepted explanation to date. The key issue is whether the increased heating rate could yield a higher REX temperature and thus cause grain refinement. Atkinson [13–14] reported lower hardness in low-carbon steels after FP at a higher heating rate due to lower REX onset temperature. However, more recent research has suggested that a higher heating rate could increase the REX onset temperature in both ultralow/low carbon steels [15–17] and IF steel [18]. Moreover, Reis *et al.* [19] observed the saturation of grain refinement in severely deformed IF steel when the heating rate exceeded 1000°C/s. In this paper, as-received commercial cold-rolled IF steel was

Corresponding author: Hai-wen Luo E-mail: luohaiwen@ustb.edu.cn

subjected to two different FPs, the first being direct heating to the target peak temperature at a rate of either 200°C/s or 500°C/s, and the other including a preheating stage prior to ultrafast heating to the peak temperature. The REX behavior during these two FPs and the resultant mechanical performances were then studied to resolve this dispute.

2. Experimental

A 0.8-mm-thick sheet of as-received IF commercial cold-rolled steel was obtained from the steel industry and subjected to a 60% cold-rolled reduction in thickness. The chemical composition of the sheet was C 0.0015wt%, Si 0.01wt%, Mn 0.1wt%, Al 0.03wt%, Ti 0.02wt%, and Fe Bal. From this sheet, we cut specimens for the FP experiment with the dimensions 20 mm × 100 mm, with the length parallel to the rolling direction. Some were directly heated at a rate of 200 or 500°C/s to designated peak temperatures and then immediately water quenched, i.e., single-stage FP. Others were subjected to two-stage FP, i.e., first being preheated to 400°C at a rate of 5°C/s and then heated to different peak temperatures at a rate of 200°C/s. To trace the REX kinetics associated with both FPs, peak temperatures were chosen at intervals of 25°C between 700 and 800°C and at intervals of 15°C between 840 and 870°C, as shown in Fig. 1. We performed single-stage FPs with peak temperatures at 715 and 725°C and two-stage FP at 720 and 730°C, as they each lead to about a 50% recrystallized fraction. For comparison, another specimen was heated in a box furnace to 870°C for 5 min to simulate the continuous annealing (CA) process. All the FPs were performed on a Gleeble-1500 thermomechanical simulator, in which a temperature distribution with a deviation of less than 5°C could be achieved in the 30 mm zone in the middle of the specimen, based on previous temperature measurements by three thermocouples. The above heating processes to 870°C were termed 200–870 and 500–870 for the single-stage FPs, P870 for the two-stage FP, and CA870 for the CA process.

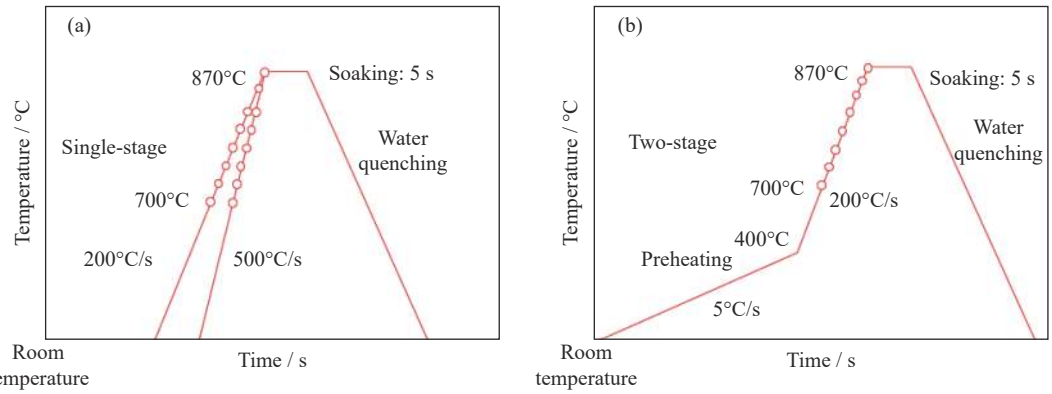

Fig. 1. Schematic illustration of the different flash processes employed: (a) single-stage FPs with a heating rate of 200 or 500°C/s; (b) two-stage FP with the imposed preheating stage.

The evolution of the micro-hardness of the samples during FP, which were deliberately interrupted during different FPs to 870°C (see Fig. 1), was traced using a micro-hardness tester (FM300) at a loading of 1.96 N with a dwell time of 10 s. Uniaxial tensile tests were conducted at a strain rate of $6.67 \times 10^{-4}\ s^{-1}$ on a WDW-200D tensile testing machine, using ASTM-E8/E8M standard samples with a gauge length of 25 mm.

Before and after these heat treatments, the microstructures of the samples were examined by optical microscopy (OM) after being etched in 4vol% nitric alcohol for 10 s after standard mechanical polishing. Next, on samples that had been subjected to electropolishing in 20vol% alcohol perchlorate, electron back-scattered diffraction (EBSD) measurements were performed using a Scanning Auger Nanoprobe, PHI710, with an angular accuracy of 0.1° at an accelerated voltage of 20 kV and a step size of 0.5 μm. EBSD examinations were made on the plane perpendicular to the transverse direction (TD) with the area of about 0.03 mm^2 near the half-thickness region of the specimen. All the EBSD data were processed using EDAX OIM software and its clean-up function for grain dilation at a 5° grain-tolerance angle, level 2 minimum grain size, and a single iteration. The orientation distribution function (ODF) was calculated using a step size of 5°. Kernel average misorientation (KAM) mapping was conducted by selecting the first nearest neighbor and an upper cut of limit of less than 5° misorientation. In addition, the low-angle and high-angle grain boundaries were defined as boundary misorientation angles lower and higher than 15°, respectively.

3. Results

3.1. Initial cold-rolled microstructure

We examined the as-received cold-rolled microstructure in the section perpendicular to the TD near the half-thickness, as shown in Fig. 2. Shear bands were observed between the layers of elongated grains (Fig. 2(a)) due to the severe de-

formation, which formed via dislocation glide and rigid-body rotation [20]. These were mostly located in γ-fiber (ND//{111}) grains, which are blue in Fig. 2(a), with a small fraction of orange and purple α-fiber (RD (rolling direction)//<110>) grains [21] in the figure, which deviate from the longitudinal rolling direction by 20°–40°. This is consistent with a previous finding that γ-fiber forms more easily than α-fiber at the initial stage of cold rolling [22]. We note that just a few {110}<uvw> grains also appear in the cold-rolled microstructure, which are colored green in Fig. 2(a). Comparison of the ODF at Euler angle φ_2 = 45° (Fig. 2(b)) with the ideal positions of the α texture in bcc steel (Fig. 2(c)) also reveals both γ-fiber and α-fiber, whose strongest texture components are at {111}<011> and {112}<110> respectively, with intensity values greater than 8.88 multiples of random density (mrd).

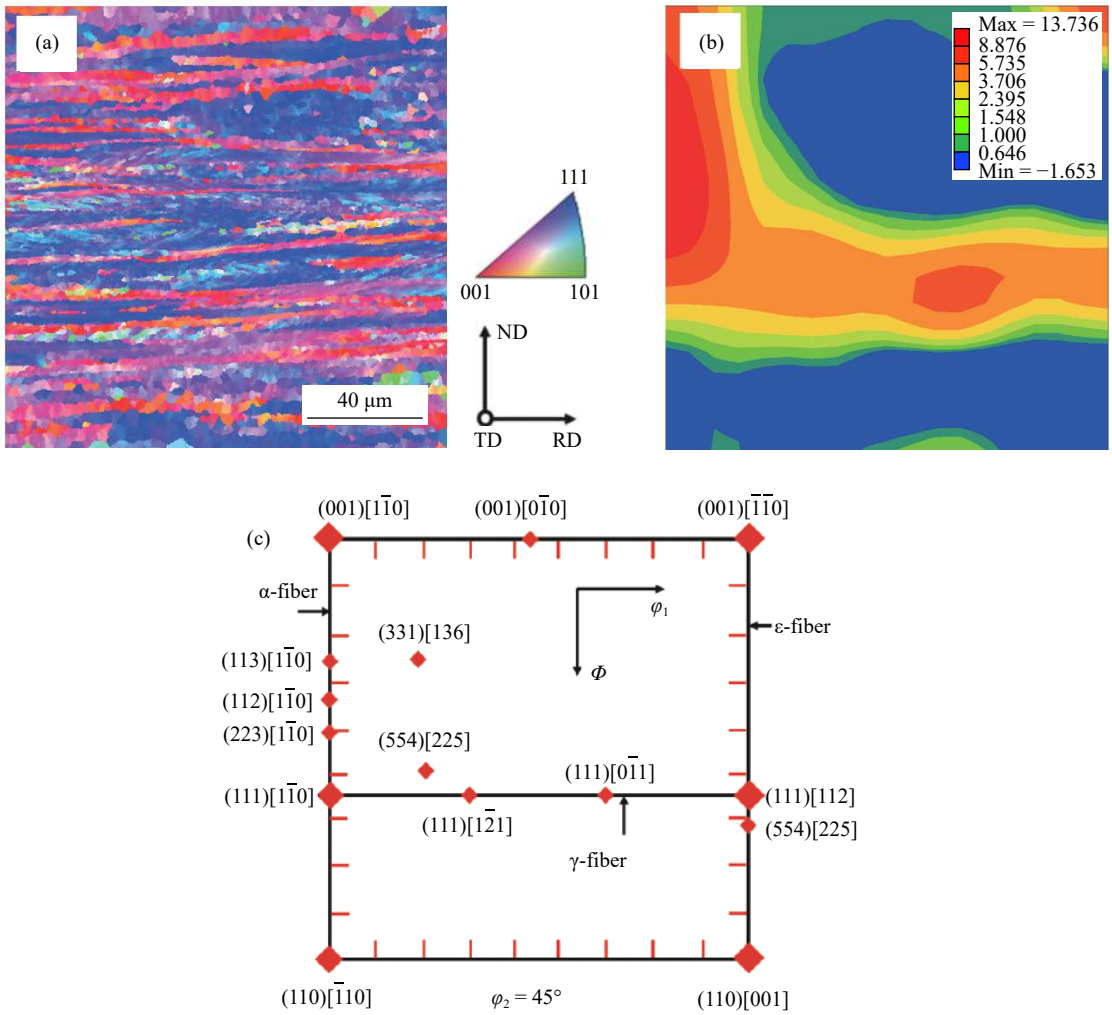

Fig. 2. (a) EBSD normal direction-inverse pole figure (ND-IPF) for orientation mapping, (b) ODF images at φ_2 = 45° for the cold-rolled IF steel, and (c) the ideal positions of some important bcc texture components at the φ_2 = 45° section of the Euler space. In particular, φ_1, φ_2, and Φ are Euler angles with the TD, ND, and RD in the crystal axis system, respectively.

3.2. Recrystallization evolution and tensile properties

To trace the REX kinetics, we measured the micro-hardness of the samples heated to different peak temperatures at the same rate. The average value was taken from ten measurements for each sample. We calculated the recrystallized fraction, X_T, as reported by [23–24]:

$$X_T = \frac{H_{max} - H_T}{H_{max} - H_{min}} \quad (1)$$

where H_{max} is the hardness of cold-rolled IF steel in the as-received state, H_{min} is the hardness in a fully recrystallized state, and H_T is the hardness of a sample heated to different peak temperatures prior to full REX.

Fig. 3(a) shows the measured recrystallized fraction as a function of peak temperature (T) for the different FP routines together with the correspondent fittings with high correlation coefficients. The temperatures for the 50% (T_{50}) and 100% (T_{100}) recrystallized fractions in the different FPs could be

then precisely determined from these fitting curves. The heating rate in the single-stage FP had a negligible influence on the REX temperature, but preheating clearly led to the increase of T_{50} by about 15°C and of T_{100} by about 40°C (see Fig. 3(a)). Fig. 3(b) shows the grain size distributions in the fully recrystallized samples, measured on about 500 grains, and the detailed value of average sizes are listed in Table 1. We can clearly see that when all specimens were heated to 870°C, all the FP routines led to larger fraction of fine grains and smaller average grain sizes than obtained in the CA process. In particular, the increased heating rate from 200°C/s to 500°C/s had a negligible effect on grain refinement, whereas use of the preheating stage produced the finest grain size, see Table 1.

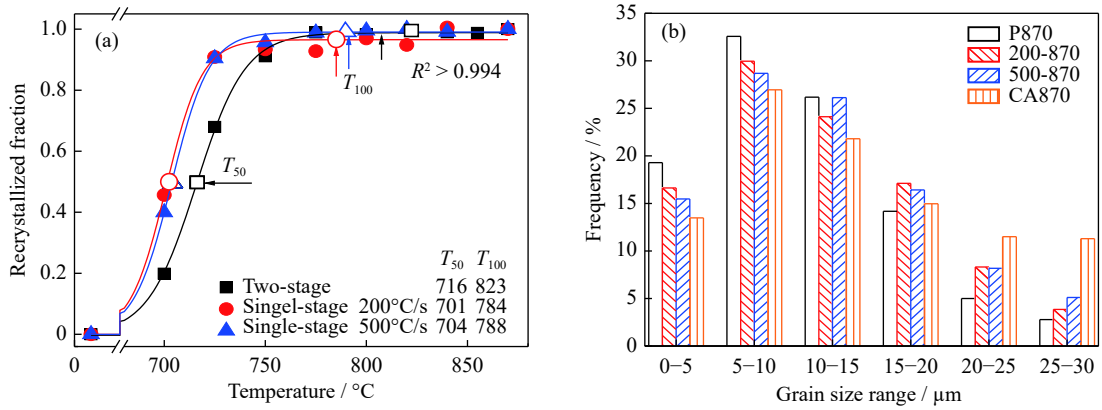

Fig. 3. (a) Recrystallized fraction as a function of peak temperatures for different heating processes and (b) the resultant grain size distribution in the fully recrystallized specimens after heating to 870°C.

Table 1. Measured average grain sizes in the fully recrystallized specimens after heating to 870°C with different heating processes

Heating process	Average grain size / μm
P870	10.8 ± 6.2
200-870	12.0 ± 7.0
500-870	11.8 ± 6.7
CA870	14.0 ± 8.9

Fig. 4 shows the measured tensile properties, which clearly reveal that increasing the peak temperature can lead to decreases in the both yield strength (YS) and ultimate tensile strength (UTS), and increases in both the total elongation (TE) and uniform elongation (UE). This is apparently because higher temperature promotes recovery and REX, as expected [8,25–27]. Compared to the CA process, single-stage FPs to 870°C at rates of 200 and 500°C/s resulted in increases of YS by about 13.9% and 23.2%, respectively. The best mechanical properties were obtained in the 500-870 specimen, including a UTS value of 299 MPa, a YS of 147 MPa, and a TE of 43%. This demonstrates the great advantage of FP in further improving the mechanical properties of cold-rolled steel sheets in addition to unprecedented high efficiency. In contrast, two-stage FP that includes a preheating stage led to the expected higher strength but much lower ductility, as shown in Fig. 4, which was not expected.

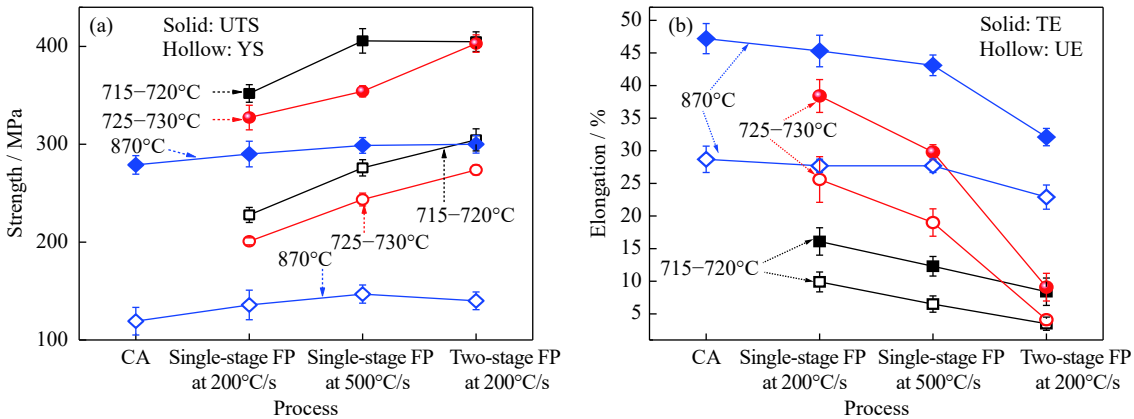

Fig. 4. Comparison in engineering properties of IF steel after heating with varied routines, including single-stage FPs at 200 and 500°C/s, two-stage FP at 200°C/s, and the CA process: (a) yield strength (YS) and ultimate tensile strength (UTS); (b) total elongation (TE) and uniform elongation (UE).

3.3. Microstructural and textural examinations

Extensive EBSD characterizations of the IF steels were made to examine their microstructural evolution during the different FP processes. Fig. 5 shows the REX process during the single- and two-stage FPs, in which the recrystallized grain boundaries are high angled [28] and marked in black.

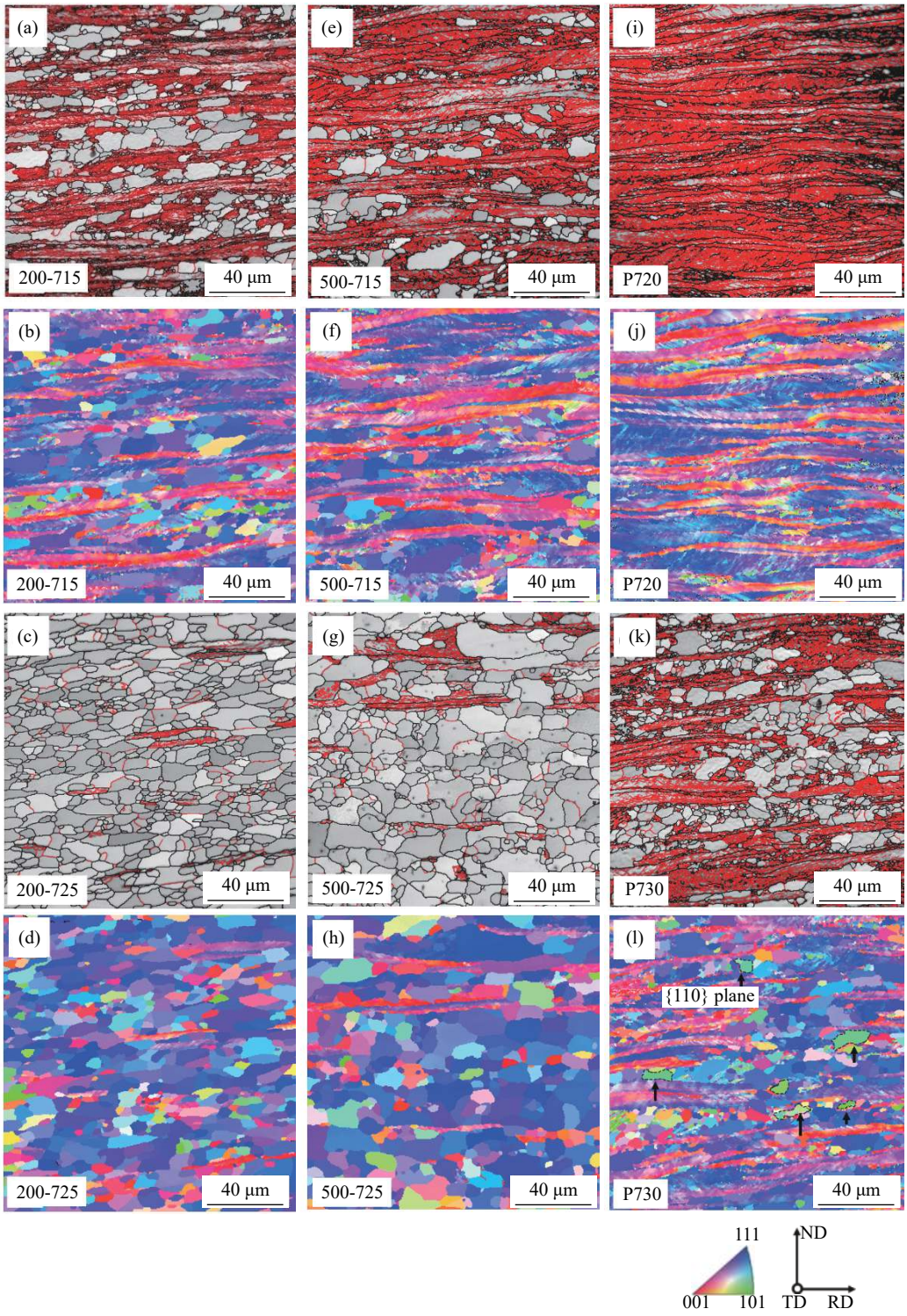

Fig. 5. EBSD image quality (IQ) overlapped with boundary mapping (GB) and ND-IPF on cold IF steel specimens heated to various peak temperatures by different processes: (a, b) 200-715; (c, d) 200-725; (e, f) 500-715; (g, h) 500-725; (i, j) P720; (k, l) P730. The {110} fiber is indicated by the dashed line in (l); low-angle grain boundaries having 0–15° misorientation are shown in red and high-angle grain boundaries with angles greater than 15° are in black in the IQ + GB maps.

When the cold-rolled IF steel was directly heated to 725°C at a rate of either 200 or 500°C/s, a much larger REX fraction was produced than that heated to 715°C (see Figs. 5(a)–5(h)), which suggests that 725°C is the critical temperature for the recrystallization of most of the cold deformed microstructure. According to the ND-IPF maps in Fig. 5, most of the recrystallized grains were located in γ-fiber, which is independent of the processing routine. Moreover, a higher heating rate clearly retarded REX. In particular, the introduced preheating stage more strongly inhibited REX, leading to much fewer REX nuclei in the P720 specimen. We also note that the partially recrystallized grains are oriented around the {110} fiber (in green), as shown by the dashed line in Fig. 5(l), which suggests that preheating may affect the nuclei orientation during REX. These evolutions are consistent with the REX kinetics depicted in Fig. 3(a).

Fig. 6 shows the ODF maps of the partially recrystallized specimens that were heated to similar temperatures using different processes. Faster heating was expected to lead to greater suppression of REX, and a higher intensity retention of the cold rolled texture in 500-725 than 200-725 specimens. In the 200-725 sample, the γ texture is concentrated at {554}<225> and {111}<112>, with the largest value being 7.48 mrd. Figs. 6(c) and 6(d) show that the texture components in specimens P720 and P730 are similar to a cold-rolled texture. Moreover, the increase in the peak temperature from 720 to 730°C led to a stronger γ-fiber in the P730 sample. Some grains in the P730 specimen have an orientation near {110}<110>, which was not found in the cold-rolled and single-stage FP specimens shown in Figs. 2 and 6. This indicates that the preheating introduced in two-stage FP may change the nuclei orientation of REX.

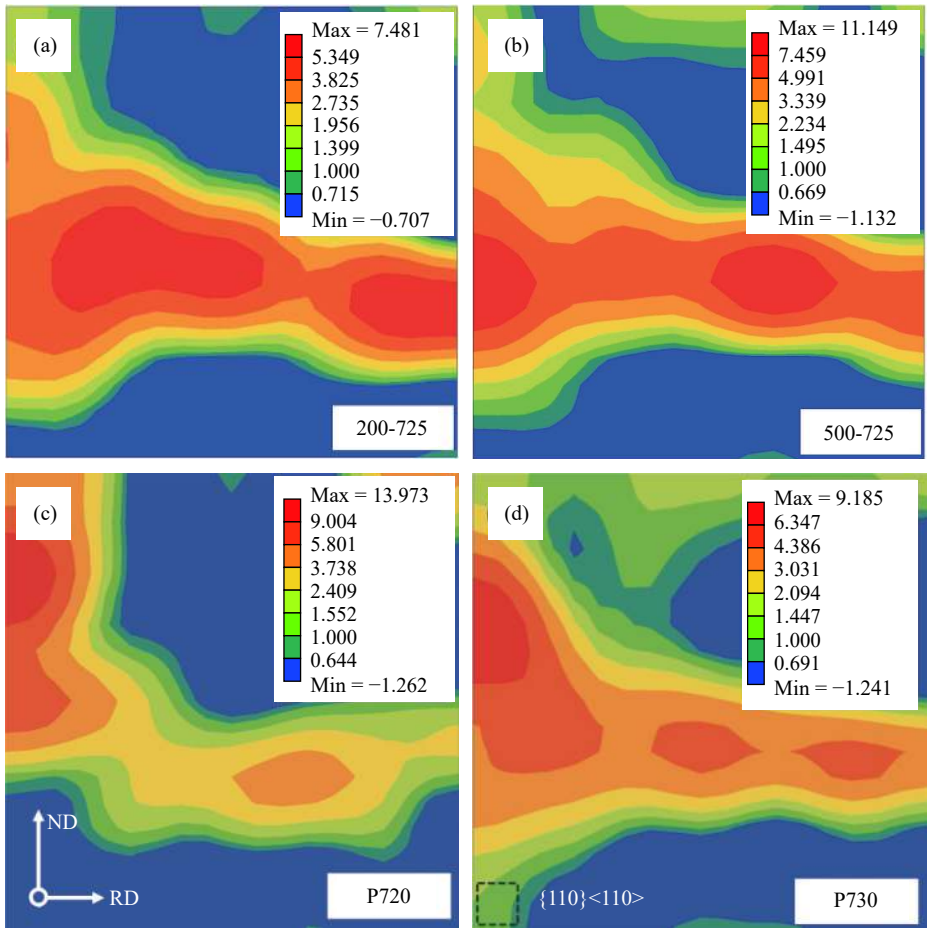

Fig. 6. ODF maps at $\varphi_2 = 45°$ of partially recrystallized microstructures in the 200-725 (a), 500-725 (b), P720 (c), and P730 (d) specimens. {110}<110> orientation is indicated by the dashed box in (d).

Fig. 7 shows the orientation densities near the ε-fiber (TD//<110>), α-fiber (RD//<110>), and γ-fiber (ND//{111}) in both the cold-rolled and fully recrystallized microstructures, with the latter achieved by heating to 870°C via different routines. After REX, the dominant α texture component in the cold-rolled microstructure vanished, whereas the γ-fiber was enhanced, which suggests that some α-fiber grains may be consumed during the formation of γ-fiber grains during REX. The fastest heating process in the single-stage FP led to the formation

of the strongest γ fiber in the 500-870 sample, which was centered at {111}<110>. In contrast, either the imposed preheating or lower heating rate led to a weaker γ-fiber with a more widely spread orientation. The strongest {110}<110> component was found in the P870 sample, which presumably resulted from the imposed preheating stage, which is in a good agreement with the micro-texture results for sample P730 in Figs. 5(l) and 6(d).

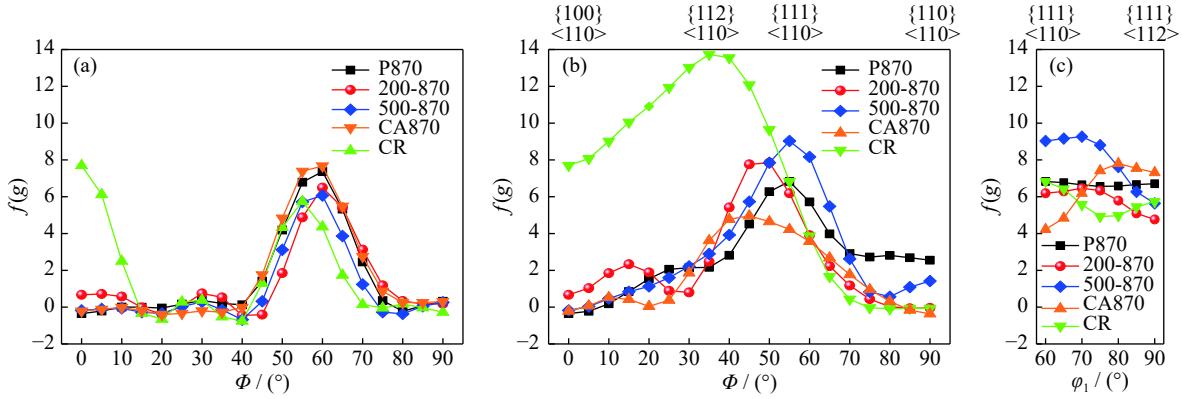

Fig. 7. Orientation densities *f*(*g*) of ε fiber (a), α fiber (b), and γ fiber (c) textures in the cold-rolled IF steel heated to 870°C by different processes. CR means the sample of received cold-rolled IF steel before heating.

We examined both the microstructures and textures after the tensile fracture of the 200-870 and P870 specimens, and observed that a higher density of geometrically necessary dislocations (GNDs) had developed in the 200-870 specimen with a corresponding higher strain concentration than that of the P870 specimen, as shown in Figs. 8(a)–8(f). This is primarily because the former experienced a larger fracture strain. From the KAM maps of Figs. 8(c) and 8(f), we can see

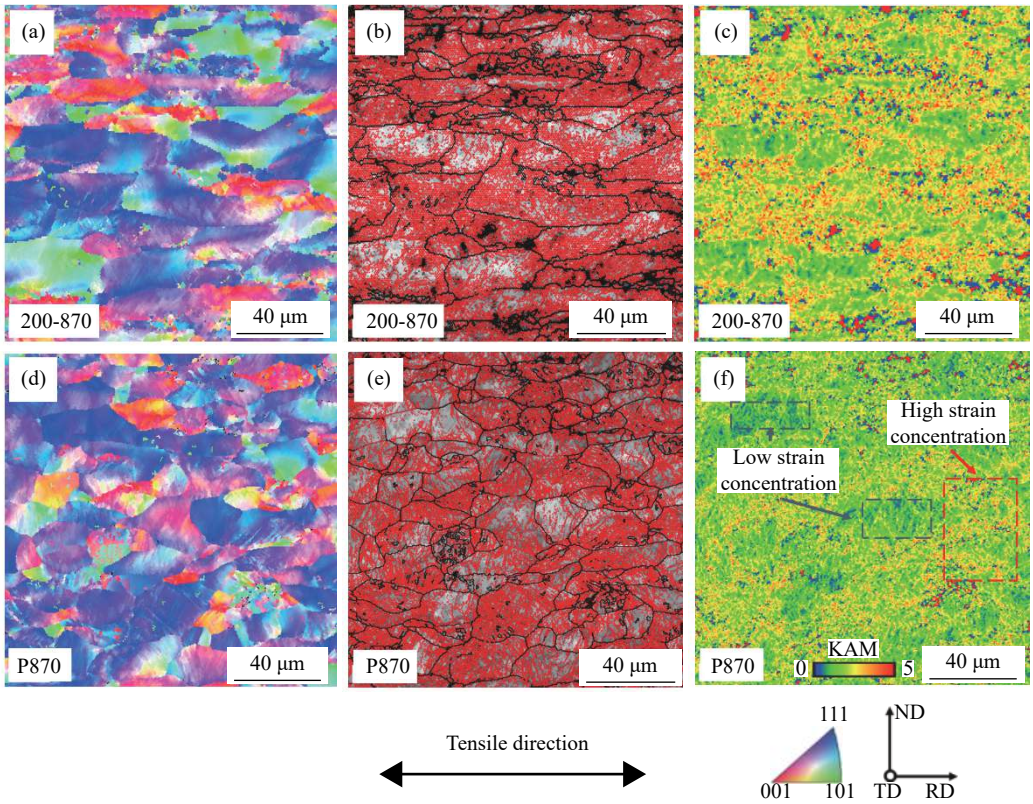

Fig. 8. Comparison of EBSD microstructures in the center of the longitudinal section after the tensile fracture of 200-870 and P870 samples: (a, d) ND-IPF figure, (b, e) IQ+GB maps, (c, f) kernel average misorientation (KAM) maps. (a, b, c) 200-870 and (d, e, f) 870 samples. Red and dark blue colors in (f) represent high and low strain concentrations, respectively. Low-angle grain boundaries with 0–15° misorientation are in red and high-angle grain boundaries with angles greater than 15° are in black in the IQ+GB maps.

that many {111}<uvw> oriented grain interiors had been subjected to a relatively low strain localization.

4. Discussion

4.1. Influence of heating rate and preheating stage on REX

The above experimental results can be summarized as follows. First, compared to the traditional CA process, all the FPs produced finer grains, which was clearly due to the much short time available for grain growth. Second, increasing the heating rate from 200 to 500°C/s had little influence on the REX temperature, but the introduction of preheating in the two-stage FP significantly increased the REX temperature, further refined the recrystallized grains, and produced a stronger {110}<110> texture component than single-stage FP.

Preheating is thought to promote active recovery prior to REX. As a consequence, the stored strain energy is greatly reduced, which leads to a lower driving force for subsequent REX and an increase in the REX temperature.

We measured the fractions of α-fiber and γ-fiber with deviations less than 15°, both of which include the components defined by the authors in Refs. [29–30], and the {110}<110> texture, the results of which are shown in Fig. 9. These results clearly reveal that a larger fraction of γ-fiber formed at the expense of α-fiber. This is actually consistent with the previous results of extensive studies of the REX annealing of cold-rolled IF steel [31–32]. The most popular theory for the formation of REX texture is either oriented nucleation [33–34] or selective growth [35]. The oriented nucleation theory assumes that strain-free REX nuclei are prevalent in grains with a particular orientation. The selective growth theory is based on observations of the preferred growth of grains

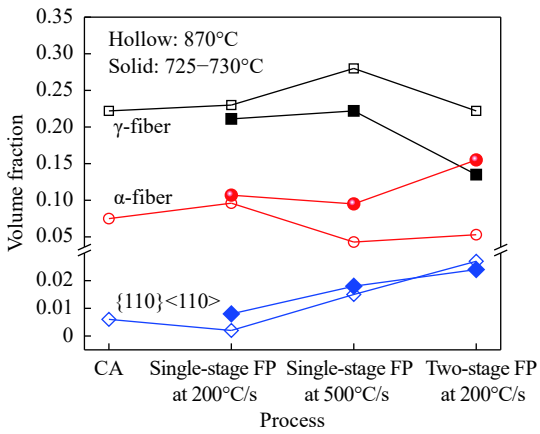

Fig. 9. Fractions of α-fiber, γ-fiber, and {100} <110> with 15° deviation after different heating processes. α-fibers include {112}<110>, {113}<110>, {114}<110>, {445}<110>, and {223}<110>; γ-fibers include {111}<112>, {111}<123>, {111}<134>, {111}<110>, and {554}<225>.

with a specific orientation from a randomly oriented array of nuclei [35].

It has been widely reported that early nucleation preferentially occurs around {110} and {111} orientations with relatively high stored strain energy [3,33,36–37]. However, both experimental and modeling results regarding the texture change during the static REX of IF steel indicated that {110}<110> fiber is prominent in the nucleation texture but is gradually eliminated in the growth texture due to its very limited growth capability [32]. According to the texture modeling results, the nucleation probability increases with increased stored strain energy of the components, whereas the growth probability of a particular orientation is determined by the inclination angle between the axis <uvw>, which relates the nucleus to the matrix, and the <110> axis, which is perpendicular to the most active slip system in ferrite [32]. Thus, the calculated growth probability along α-fiber is highest at an angle of 20° but gradually decreases with higher angles up to 90° (along the left axis of Fig. 2(c)), which is near {110}<110>, as shown in Fig. 8 in Ref. [32]. This phenomenon is consistent with the observation that the {110}<110> fraction decreases with increases in the peak temperature for all FPs except for the two-stage FP, as shown in Fig. 9.

Surprisingly, it now appears that the two-stage FP used in this study could produce about 2.7vol% {110}<110> texture components in the P870 sample. Even the single-stage FP at 500°C/s produced about 1.5vol% {110}<110> texture and the γ texture of up to 28vol% in the 500-870 specimen, as shown in Fig. 9. This is probably due to the much shorter duration of recrystallization due to faster heating or the greatly increased recrystallization temperature as compared to the conventional CA process. Thus, the prominent nucleation texture of {110}<110> could not be eliminated in time and still remained even after REX. This may be confirmed by the presence of some remaining {110} orientation grains after partial REX at lower temperature, as shown in Fig. 5(l). Moreover, the sharpened γ texture might relate to the reserved higher stored strain energy due to rapid heating, which could provide a greater driving force for the extensive seeding of high-energy γ-oriented grains.

4.2. Effects of heating rate and preheating stage on mechanical performance

As noted above, the comparison of the CA-870, 200-870, and 500-870 specimens indicates that FP can manufacture stronger and more ductile cold-rolled IF steel with unprecedented efficiency. However, use of a preheating stage during FP, which has been introduced to relieve the thermal stress and realize more precise shape control, slightly increases strength but causes unavoidable deterioration of the ductility. The increased strength can be ascribed to the refinement of the recrystallized grains, which however cannot fully explain

the deterioration in plasticity.

During deformation, dislocation movement has been found to comprise three steps: 1) extensive formation of cell walls that consist of abundant GNDs oriented at an angle of 20°–40° with the rolling direction; 2) at intermediate strain levels, the substructures are broken up, followed by the onset of new slip activity that can produce micro-shear bands; 3) at high strain levels, a boundary morphology forms with complete lamellar dislocation [22]. Generally, slips in the BCC structure can easily occur in closely packed planes, i.e., the {110}, {112}, and {123} planes. In addition, Li *et al.* [22] found that, in cold-rolled IF steel, dislocation walls compromised by GNDs were mostly parallel to the {110} plane with micro-shear bands parallel to the {112} plane. Thus, the authors suggested that slip might first proceed from the {110} plane to the {112} plane at intermediate strain, and the establishment of a new slip system in an existing dislocation structure might lead to strain localization, thereby causing a significant reduction in ductility.

Humphreys and Hatherly [38] found that the choice of slip plane in bcc metals was affected by the temperature of deformation. At temperatures below a quarter of melting temperature (T_m/4), slip occurs at {112}; between T_m/4 and T_m/2, the occurrence of slip favors {110}; at temperatures above T_m/2, slip at {123} is preferred. This means that the deformation of {110} texture becomes difficult when tensile deformation is performed at room temperature. In this case, as shown in Fig. 9, the highest volume fraction of the {110}<110> orientation is obtained in the P870 sample, which would contribute to the observed decrease in ductility due to the severe strain localization (see Fig. 8(f)) and then lead to earlier necking than occurs in other specimens. Moreover, it is generally believed that the stronger is the γ (ND//{111}) texture, the stronger anti-thinning ability can be achieved, which could simultaneously benefit deep drawing. In contrast, even though about 1.5vol% of {110}<110> fiber also formed in the 500-870 specimen, ductility is rarely affected, which might be due to its sharper γ texture components that have great resistance to early strain localization [39–40].

5. Conclusions

In this study, single- and two-stage flash processings (FPs) were employed to anneal commercial cold-rolled IF steel, and the following conclusions can be drawn.

(1) In comparison with continuous annealing at 870°C, both single- and two-stage FPs were able to refine recrystallized grain sizes, which led to increases in yield strength of more than 13.9% and 23.2% and reasonable ductility at rates of 200°C/s and 500°C/s, respectively.

(2) The imposed preheating stage in two-stage FP could increase the REX temperature higher than that achieved by the increased heating rate of single-stage FP, however, it also deteriorated the ductility. Compared to single-stage FP, two-stage FP produced a larger fraction of {110}<110> and a smaller fraction of γ texture, which might favor strain localization and lead to earlier necking and deterioration of ductility.

(3) In summary, single-stage FP, rather than two-stage FP including preheating, is recommended for the future industrial production of cold-rolled IF steel due to its high production efficiency and significantly improved mechanical properties of the resulting IF steel.

Acknowledgements

This work was financially supported by the National Natural Science Foundation of China (Nos. 51861135302 and 51831002) and Fundamental Research Funds for the Central Universities, China (No. FRF-TP-18-002C2).

References

[1] R.K. Ray, J.J. Jonas, and R.E. Hook, Cold rolling and annealing textures in low carbon and extra low carbon steels, *Int. Metall. Rev.*, 39(1994), No. 4, p. 129.

[2] I. Samajdar, B. Verlinden, L. Kestens, and P. Van Houtte, Physical parameters related to the developments of recrystallization textures in an ultra low carbon steel, *Acta Mater.*, 47(1998), No. 1, p. 55.

[3] Y. Hayakawa and J.A. Szpunar, Modeling of texture development during recrystallization of interstitial free steel, *Acta Mater.*, 45(1997), No. 6, p. 2425.

[4] C.Y. Qiu, L. Li, L.L. Hao, J.G. Wang, X. Zhou, and Y.L. Kang, Effect of continuous annealing temperature on microstructure and properties of ferritic rolled interstitial-free steel, *Int. J. Miner. Metall. Mater.*, 25(2018), No. 5, p. 536.

[5] Y.F. Shen, W.Y. Xue, Y.D. Wang, Y.D. Liu, and L. Zuo, Tensile behaviors of IF steel with different cold-rolling reductions, *Mater. Sci. Eng. A*, 496(2008), No. 1-2, p. 383.

[6] R. Wang, Y.P. Bao, Z.J. Yan, D.Z. Li, and Y. Kang, Comparison between the surface defects caused by Al_2O_3 and TiN inclusions in interstitial-free steel auto sheets, *Int. J. Miner. Metall. Mater.*, 26(2019), No. 2, p. 178.

[7] R. Wang, Y.P. Bao, Y.H. Li, Z.J. Yan, D.Z. Li, and Y. Kang, Influence of metallurgical processing parameters on defects in cold-rolled steel sheet caused by inclusions, *Int. J. Miner. Metall. Mater.*, 26(2019), No. 4, p. 440.

[8] L. Zhang, Z. Chen, Y.H. Wang, G.Q. Ma, T.L. Huang, G.L. Wu, and D.J. Jensen, Fabricating interstitial-free steel with simultaneous high strength and good ductility with homogeneous layer and lamella structure, *Scripta Mater.*, 141(2017), p. 111.

[9] M.X. Yang, Y. Pan, F.P. Yuan, Y.T. Zhu, and X.L. Wu, Back stress strengthening and strain hardening in gradient structure, *Mater. Res. Lett.*, 4(2016), No. 3, p. 145.

[10] R. Saha and R.K. Ray, Formation of nano- to ultrafine grains in a severely cold rolled interstitial free steel, *Mater. Sci. Eng. A*, 459(2007), No. 1-2, p. 223.

[11] Q.G. Meng, J. Li, and H.X. Zheng, High-efficiency fast-heating annealing of a cold-rolled dual-phase steel, *Mater. Des.*,

58(2014), p. 194.
[12] F.M. Castro Cerda, C. Goulas, I. Sabirov, L.A.I. Kestens, and R.H. Petrov, The effect of the pre-heating stage on the microstructure and texture of a cold rolled FeCMnAlSi steel under conventional and ultrafast heating, *Mater. Charact.*, 130(2017), p. 188.
[13] M. Atkinson, Bifurcation of thermal restoration processes in deformed iron and steel, *Mater. Sci. Eng. A*, 262(1999), No. 1-2, p. 33.
[14] M. Atkinson, On the credibility of ultra rapid annealing, *Mater. Sci. Eng. A*, 354(2003), No. 1-2, p. 40.
[15] D. Muljono, M. Ferry, and D.P. Dunne, Influence of heating rate on anisothermal recrystallization in low and ultra-low carbon steels, *Mater. Sci. Eng. A*, 303(2001), No. 1-2, p. 90.
[16] M. Ferry, D. Muljono, and D.P. Dunne, Recrystallization kinetics of low and ultra low carbon steels during high-rate annealing, *ISIJ Int.*, 41(2001), No. 9, p. 1053.
[17] F.M. Castro Cerda, F. Vercruysse, T.N. Minh, L. Kestens, A. Monsalve, and R. Petrov, The effect of heating rate on the recrystallization behavior in cold rolled ultra low carbon steel, *Steel Res. Int.*, 88(2017), No. 1, p. 1600351.
[18] L. Kestens, A.C.C. Reis, W. Kaluba, and Y. Houbaert, Grain refinement and texture change in interstitial free steels after severe rolling and ultra-short annealing, *Mater. Sci. Forum*, 467-470(2004), p. 287.
[19] A.C.C. Reis, L. Bracke, R. Petrov, W.J. Kaluba, and L. Kestens, Grain refinement and texture change in interstitial free steels after severe rolling and ultra-short annealing, *ISIJ Int.*, 43(2003), No. 8, p. 1260.
[20] Q.Z. Chen, M.Z. Quadir, and B.J. Duggan, Shear band formation in IF steel during cold rolling at medium reduction levels, *Philos. Mag.*, 86(2006), No. 23, p. 3633.
[21] Z.Y. Hou, Y.B Xu, and D. Wu, Recrystallization of ultra-low carbon steel sheet after ultra-rapid annealing, *Acta Metall. Sin.*, 48(2012), No. 9, p. 1057.
[22] B.L. Li, A. Godfrey, Q.C. Meng, Q. Liu, and N. Hansen, Microstructural evolution of IF-steel during cold rolling, *Acta Mater.*, 52(2004), No. 4, p. 1069.
[23] S. Dziaszyk, E.J. Payton, F. Friedel, V. Marx, and G. Eggeler, On the characterization of recrystallized fraction using electron backscatter diffraction: A direct comparison to local hardness in an IF steel using nanoindentation, *Mater. Sci. Eng. A*, 527(2010), No. 29-30, p. 7854.
[24] J.L. Bocos, E. Novillo, M.M. Petite, A. Iza-Mendia, and I. Gutierrez, Aspects of orientation-dependent grain growth in extra-low carbon and interstitial-free steels during continuous annealing, *Metall. Mater. Trans. A*, 34(2003), No. 3, p. 827.
[25] A. Smith, H.W. Luo, D.N. Hanlon, J. Sietsma, and S. Van Der Zwaag, Recovery processes in the ferrite phase in C–Mn steel, *ISIJ Int.*, 44(2004), No. 7, p. 1188.
[26] H.W. Luo, J. Sietsma, and S. Van Der Zwaag, Effect of inhomogeneous deformation on the recrystallization kinetics of deformed metals, *ISIJ Int.*, 44(2004), No. 11, p. 1931.
[27] H.W. Luo, Comments on "Austenite stability of ultrafine-grained transformation-induced plasticity steel with Mn partitioning" by S. Lee, S.J. Lee and B.C. De Cooman, *Scripta Mater.*, 66(2012), No. 10, p. 829.
[28] F. Yang, H.W. Luo, E.X. Pu, S.L. Zhang, and H. Dong, On the characteristics of Portevin–Le Chatelier bands in cold-rolled 7Mn steel showing transformation-induced plasticity, *Int. J. Plast.*, 103(2018), p. 188.
[29] R. Saha and R.K. Ray, Texture and grain growth characteristics in a boron added interstitial free steel after severe cold rolling and annealing, *Mater. Sci. Eng. A*, 527(2010), No. 7-8, p. 1882.
[30] R. Saha and R.K. Ray, Effect of severe cold rolling and annealing on the development of texture, microstructure and grain boundary character distribution in an interstitial-free (IF) steel, *ISIJ Int.*, 48(2008), No. 7, p. 976.
[31] K. Shen and B.J. Duggan, Microbands and crystal orientation metastability in cold rolled interstitial-free steel, *Acta Mater.*, 55(2007), No. 4, p. 1137.
[32] L. Kestens and J.J. Jonas, Modeling texture change during the static recrystallization of interstitial-free steels, *Metall. Mater. Trans. A*, 27(1996), No. 1, p. 155.
[33] R.L. Every and M. Hatherly, Oriented nucleation in low-carbon steels, *Texture*, *Stress*, *Micro.*, 1(1974), art. No. 380237.
[34] I.L. Dillamore, C.J.E. Smith, and T.W. Watson, Oriented nucleation in the formation of annealing textures in iron, *Met. Sci. J.*, 1(1967), No. 1, p. 49.
[35] K. Verbeken, L. Kestens, and J.J. Jonas, Microtextural study of orientation change during nucleation and growth in a cold rolled ULC steel, *Scripta Mater.*, 48(2003), No. 10, p. 1457.
[36] D. Vanderschueren, N. Yoshinaga, and K. Koyama, Recrystallisation of Ti IF steel investigated with electron backscattering pattern (EBSP), *ISIJ Int.*, 36(1996), No. 8, p. 1046.
[37] W.B. Hutchinson, Development of textures in recrystallization, *Met. Sci.*, 8(1974), No. 1, p. 185.
[38] F.J. Humphreys and M. Hatherly, *Recrystallization and Related Annealing Phenomena*, 2nd ed., Elsevier Science Ltd., Oxford, 2004, p. 25.
[39] C.I. Xie, E. Nakamachi, and X.H. Dong, Study of texture effect on strain localization on bcc steel sheets, *Acta Mech. Solida Sin.*, 13(2000), No. 2, p. 95.
[40] C.L. Xie and E. Nakamachi, The effect of crystallographic textures on the formability of high-strength steel sheets, *J. Mater. Process. Technol.*, 122(2002), No. 1, p. 104.